Magnetic order and defect structure of Fe_xAl_{1-x} alloys around $x=0.5$: An experimental and theoretical study

J. Bogner, W. Steiner, and M. Reissner
Institut für Angewandte und Technische Physik, TU Wien, A-1040 Wien, Austria

P. Mohn, P. Blaha, and K. Schwarz
Institut für Technische Elektrochemie, TU Wien, A-1060 Wien, Austria

R. Krachler and H. Ipser
Institut für Anorganische Chemie, Universität Wien, A-1090 Wien, Austria

B. Sepiol
Institut für Materialphysik, Universität Wien, A-1090 Wien, Austria

(Received 2 February 1998)

High-field ^{57}Fe Mössbauer investigations up to 13.5 T on a series of Fe_xAl_{1-x} alloys around $x=0.5$ and magnetic measurements on a 51.8% sample are performed between 4.2 and 295 K. The experimental results are complemented with augmented spherical-wave (ASW) and linear augmented plane-wave (LAPW) band structure as well as thermodynamic model calculations. For ideally ordered FeAl ($B2$ structure) both types of band-structure calculations yield $\mu_{Fe}=0.71\mu_B$. The ferromagnetic ground state is 0.7 mRy per formula unit below the nonmagnetic state. In experiment it was found that only approximately 25% of the Fe atoms carry a magnetic moment. This discrepancy can be explained if noncollinear spin ordering is allowed and a high density of defects is taken into account, which is typical for real alloys and destroys translational periodicity. Experimentally magnetic moments are only observed for Fe antistructure atoms and their eight Fe neighbors. This nine-atom cluster has a mean moment of $0.4\mu_B$ per atom, which is in fair agreement with the results from supercell (16 and 54 atoms) calculations ($0.6\mu_B$). For the Mössbauer analysis four subspectra are used, which are allocated to (i) Fe in the completely ordered $B2$ structure, (ii) Fe antistructure atoms, and (iii) their nearest Fe neighbors, as well as (iv) Fe atoms around a vacancy in the Fe sublattice. This analysis allows us to obtain simultaneously the concentration of both the Fe vacancies and the Fe antistructure atoms. The derived temperature dependence for both defect types corresponds well with thermodynamic model calculations, which account for all possible kinds of point defects.
[S0163-1829(98)05345-4]

I. INTRODUCTION

Because of their simple crystal structure and high tendency to form ordered alloys, iron aluminides around 50% Fe represent an ideal substance to study the influence of atomic order on the magnetic properties. The number and local arrangement of defects created by different heat treatments directly influence the mechanical properties.[1–4] Therefore many investigations on these technologically important alloys are reported in literature. The precise concentrations of the different defects are, however, not well known. Furthermore band-structure calculations for ordered alloys with equiatomic composition obtained a magnetic ground state, whereas most of the experimental investigations point to a vanishing Fe moment.

To contribute to a better understanding of the magnetic behavior and the characteristic defect structure we report in the present paper on detailed high-field Mössbauer investigations up to 13.5 T on a series of Fe_xAl_{1-x} alloys around $x=0.5$. The extremely local character of this method and the advantage that no additional probe atom must be diffused into the material, offers a unique possibility to study effects on the electronic structure caused by antistructure atoms or vacancies. A 51.8% Fe alloy, heat treated at 700 °C to obtain thermal equilibrium, was selected for a magnetic investigation to allow a comparison with those reported in the literature. The experimental results are combined with augmented spherical-wave (ASW) and linear augmented plane-wave (LAPW) band structure as well as thermodynamic calculations.

The ideal crystal structure of the alloys investigated is $B2$ (CsCl), which consists of two interpenetrating simple cubic lattices occupied by Fe and Al, respectively (Fig. 1). Interstitial atoms are energetically unfavorable and thus there are four possible point defects, namely, vacancies or antistructure atoms on both sublattices. On the Fe-rich side of the phase diagram it was shown (e.g., Ref. 5) that only three are predominately formed: Fe atoms substituting Al (Fe antistructure, Fe AS), vacancies on the Fe sublattice (Fe vacancy), and to a very small extent vacancies on the Al sublattice. The number of Al atoms on Fe sites (Al antistructure, Al AS) is generally found to be negligible in this part of the phase diagram. Given, that at the equiatomic composition the number of vacancies present must be equal on both sublattices, an Fe AS atom can only occur, if an Fe atom fills the Al vacancy, leaving behind an additional vacancy on the Fe

 ©1998 The American Physical Society

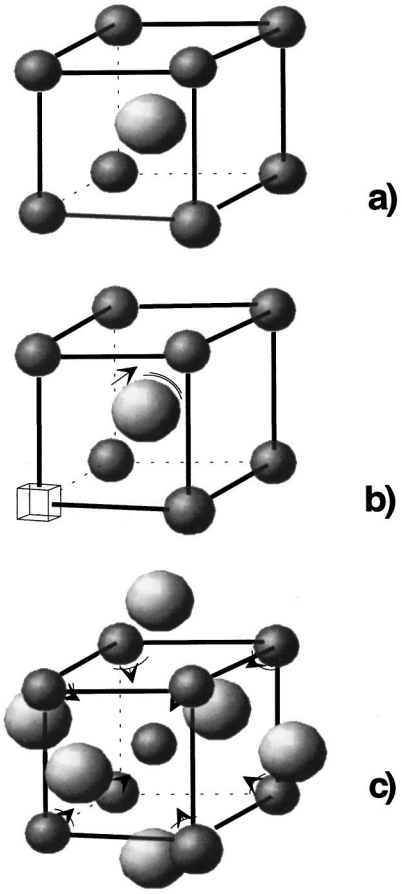

FIG. 1. (a) Schematic representation of the undistorted $B2$ structure (Al atoms, larger spheres). (b) Inclusion of an Fe vacancy. (c) Environment for an Fe AS atom. The arrows mark the relaxation of the atomic positions obtained from the LAPW calculations.

sublattice. Defects of this type are called triple defects[6] and are often assumed to be characteristic for FeAl alloys (e.g., Ref. 1).

It was reported that around $Fe_{0.5}Al_{0.5}$ the measured ^{57}Fe Mössbauer spectrum consists of only one single line[7] and that up to applied fields of 8.5 T the hyperfine field (B_{hf}) at 4.2 K was equal to the external one.[8] Recent investigations with well defined samples,[9,10] did not confirm these earlier results but rather showed a considerable line broadening, independent of the heat treatment. Lots of magnetic investigations have already been performed on samples obtained after a variety of heat treatments: In the extensive studies of Köster and co-workers[11] the Curie-Weiss contribution of the susceptibility, corrected by a temperature independent term χ_0 (extrapolated from the temperature region 300–650 K) leads to Weiss temperatures (θ) around zero. Domke and Thomas[12] obtained from the extrapolation of the low-temperature data a θ value between 0 and -2 K. Höhl[13] reported for this quantity a linear decrease with x, starting from -40 K for $x=0.5$. Parthasaranti and Beck[14] fitted their magnetic measurements by a superposition of two Langevin-type functions and ended up with a moment of $2.2\mu_B$ for Fe embedded in the Al sublattice and $29.8\mu_B$ summed up over the Fe atoms in the surrounding shells. Caskey, Franz, and Sellmyer[15] concluded from their own measurements and a critical examination of available data from the literature that completely ordered FeAl is nonmagnetic down to 1 K. Assuming, however, a nine atom cluster (Fe AS and the eight surrounding atoms) the Fe AS atoms possess a localized moment which polarize these eight surrounding Fe atoms leading to an overall moment of $7.8\mu_B$ for the cluster.

General agreement exists for the band structures and density of states (DOS) derived by different techniques.[16–20] Some hybridization between the Al s,p bands and the Fe d bands is reported, leading to a partly covalent character of the bond.[21] The charge transfer from the Al to the Fe site depends on the definition and thus on the method of calculation and ranges from 0.27 (Ref. 22) to less than 0.09 (Ref. 23) electrons. In contrast to the experiments, however, an Fe moment of 0.55 to $0.7\mu_B$ is found in the ordered equiatomic compounds.[19,22,24] The corresponding minimum in the total energy curve is only 0.7 mRy below that of the paramagnetic state, for which the Fe moment is zero.[19,22] Antistructure atoms were taken into account by scalar relativistic linear muffin-tin orbital calculations assuming ordered supercells.[24] They lead to an overlap between the d orbitals of Fe AS and the eight surrounding atoms resulting in changes of the local DOS as compared to the ordered equiatomic alloy. Depending on the size of the chosen supercell, moments between 4.88 and $7.77\mu_B$/cluster are obtained for the surrounding Fe atoms, whereas the moment of the Fe AS atom itself stays roughly constant at $2.5\mu_B$.

Comparing a variety of experimental results Köster and co-workers[11] proposed a separation of the $B2$ homogeneity range into two phases. Structural changes at the respective temperatures were, however, not observed. Frantz[25] concluded that a support of the annealing out of Fe AS atoms starts at the suggested phase boundary due to the formation of vacancies on both sublattices. Using for μ_{eff}/Fe the values deduced from the measurements of Köster and co-workers[11] ($4.0-4.6\mu_B$) as well as those reported by Domke and Thomas[12] ($5.0-5.6\mu_B$) he obtained Fe AS concentrations, which, assuming the validity of a triple defect model, led to vacancy concentrations higher than those reported in the literature, whereas with $\mu_{eff}/Fe=7.8\mu_B$ (Ref. 15) agreement was obtained. Vacancies on both sublattices (but in the nearest neighborhood) were proposed to explain the diffusion process of Fe at elevated temperatures.[10,26]

Calculations of the point defect concentrations based on statistical thermodynamic models of nearest-neighbor pairwise interactions[6,27,28,29] provide useful insight into the equilibrium conditions. Although at low temperatures a triple defect structure follows as the most likely one, inclusion of the Al vacancies improves the overall agreement between experiment and theory.[30]

In contrast to the thermodynamic approach, which is based on isolated defects, first-principle calculations[31] assume a vacancy clustering. These calculations are performed within density-functional theory (employing the local spin-density approximation) using a supercell. Although the dimensions of the supercells are small these calculations deduce defect concentrations that are much lower than those observed in experiments.[31,32] Recent investigations for $T=0$ K based on a semiempirical method[33] suggest a phase transition at $x\sim0.48$ and found a tendency for agglomeration of the Fe atoms at the Fe-rich side of the phase diagram.

TABLE I. Iron concentration and quenching temperatures as well as center shift (CS relative to the ^{57}Co**Rh** source at 4.2 K) quadrupole splitting ($eQV_{zz}/4$) and internal field [$B_{int}(T)$] at 4.2 K measured at ^{57}Fe embedded in distinct environments of the investigated samples. (Standard deviation of the Mössbauer data: ± 0.016 mm/s).

Sample	Fe concentration (at. %)	Quenching temperature (°C)	In ordered $B2$ CS 1 (mm/s)	Neighbors of Fe vacancy CS 2 (mm/s)	Neighbors of Fe vacancy $eQV_{zz}/4$ (mm/s)	Corner atoms around Fe AS CS 3 (mm/s)	Corner atoms around Fe AS B_{int} at 13.5 T	Fe AS atom CS 4[c] (mm/s)	Fe AS atom B_{int} at 13.5 T
1	51.8±0.2[a]	700	0.180	0.170	−0.14	0.144	−2.80	0.144	−6.0
2	52.2±0.3[b]	700	0.180	0.180	−0.14	0.155	−2.80	0.155	−6.0
3	50.6±0.2[a]	800	0.175	0.170	−0.14	0.135	−3.00	0.135	−5.5
4	52.5±0.3[b]	appr. 850	0.160	0.150	−0.15	0.150	−2.80	0.150	−6.2
5	51.0±0.2[a]	1000	0.185	0.170	−0.12	0.144	−3.10	0.144	−5.5
6	51.0±0.2[a]	appr. 1200	0.185	0.170	−0.09	0.144	−3.15	0.144	−6.0
7	50.6±0.2[a]	appr. 1200	0.185	0.180	−0.09	0.144	−2.90	0.144	−5.0

[a]Determined by wet chemical analysis.
[b]Determined by microprobe analysis.
[c]Constrained to CS 3.

The paper is organized as follows: Sections II and III deal with experimental details and describe the theoretical methods. Section IV gives the results and discussion, and Sec. V contains a brief summary with concluding remarks.

II. EXPERIMENTAL DETAILS

Two types of samples were investigated. One single crystal was prepared by the Czochralski method and cut perpendicular to the [111] direction. Its final composition was determined by microprobe analysis (Table I). All other samples were prepared by melt spinning. X-ray investigations confirmed them to be well crystallized and of single phase $B2$ structure. At distinct temperatures extended heat treatments followed by different cooling procedures were applied to freeze the defect structure formed at a certain temperature. In addition, two as cast (melt spun) samples were included in the present investigations since we expect that a larger number of vacancies will be retained in these specimens. The different quenching temperatures and final chemical composition determined by wet chemistry or microprobe analysis are summarized in Table I. Details of the sample preparation and heat treatments are given in Ref. 9.

^{57}Fe Mössbauer spectra were recorded in transmission geometry in the temperature interval between 4.2 and 295 K. In addition measurements in external fields (B_a) up to 13.5 T were performed at 4.2 K. The fields were produced by superconducting coils and controlled with a Hall probe. The accuracy of the field was ± 0.01 T, with a homogeneity of 0.1% over a cylinder with a height of 2 mm and a diameter of 15 mm. The source was situated in a field-compensated area (residual field less than 0.1 T). The direction of the field was parallel to the γ-ray direction. α-Fe foils were used for both experiments as velocity standards. All center shift (CS) values reported are given relative to the ^{57}Co**Rh** source at 4.2 K.

The spectra recorded at different temperatures and external fields were simultaneously analyzed by solving the complete Hamiltonian with magnetic and quadrupole splitting in the fast relaxation limit within the thin absorber approximation.[34] The finite thickness of the absorbers (especially for the thinned single crystal) was taken into account using the correction formula of Mørup and Both.[35] According to the used model the number of subspectra was kept constant and the quadrupole splitting as well as the full width at half-maximum (FWHM) of the different subspectra were assumed to be temperature independent. The CS was supposed to follow the usual second-order Doppler shift. The difference of the individual CS values was constrained to be constant. For the polycrystalline samples the different orientations of the main axis of the electric-field gradient (EFG) tensor with respect to the γ-ray direction were taken into account by a proper randomization procedure. In all fits the asymmetry parameter (η) was set to zero.

Bulk magnetic measurements in external fields up to 7 T were performed on sample 1 (Table I) with a vibrating sample magnetometer in the temperature interval 4.2 to 220 K. Ni was used for the calibration of the magnetization. The uncertainties are $\pm 1\%$ for the magnetization and ± 0.25 and ± 0.5 K for the temperature at low and high temperatures, respectively.

III. THEORETICAL CALCULATIONS

To support the experimental investigations concerning the magnetic behavior we performed calculations of the electronic properties of ordered FeAl ($B2$), and Fe-Al supercells with 16 ($2\times2\times2$), 32 ($4\times4\times4$ with defects in fcc geometry) and 54 ($3\times3\times3$) atoms, simulating various defect structures. In addition calculations for possible non-collinear-spin ordering for FeAl ($B2$) and for the 16-atom supercell containing a nine-Fe-atom cluster were carried out. These calculations employed the LAPW (Ref. 36) and the ASW (Ref. 37) method. In particular 408 **k** points for the $B2$ structure and 30 **k** points for the 54-atom supercell in the irreducible wedge of the first Brillouin zone were used. For the non-collinear-spin calculations that require very high accuracy, about 1800 **k** points were sufficient to ensure an

accuracy of the total energy better than 0.1 mRy. For all calculations the local-spin-density approximation (LSDA) for exchange and correlation was applied, but we checked also the generalized gradient approximation (GGA) (Ref. 38) and found very similar results. It should be noted that essentially the same results were obtained for both, the LAPW and the ASW method, where LAPW is a full-potential scheme (without any shape approximation on potential or charge density) but ASW uses the atomic sphere approximation (spherical average inside overlapping atomic spheres). Therefore the ASW method is much faster but can be used with confidence for the time-consuming supercell calculations including non-collinear-spin ordering (for details see Ref. 39), whereas the LAPW method was used to determine the EFG's at the Fe sites (where non-spherical charge-density components are important) and the relaxation of atoms near vacancies or antisite atoms (where the calculation of forces at the nuclei are necessary).

The temperature dependence of the defect concentration was estimated by a statistical-thermodynamic model for $B2$ phases based on the grand canonical ensemble recently presented by Krachler and Ipser.[40] This allows (in contrast to the model by Chang and Neumann[5]) to simultaneously treat isolated vacancies and antistructure atoms on both sublattices and concomitantly simplifies some of the mathematics used in earlier approaches.[30,41] The present experimental results yield for each sample with a defined composition and temperature the two different defect concentrations (Fe vacancies and Fe AS atoms) and thus allow an ideal test for these model equations (see the Appendix). The model parameters are the point defect concentrations in the exactly stoichiometric alloy at a certain temperature.

IV. RESULTS AND DISCUSSION

A. Energy band-structure calculations

The band-structure calculation for FeAl in the CsCl ($B2$) structure leads to a magnetic ground state in which the Fe atoms possess a magnetic moment of $0.71\mu_B$. A compression of the volume by more than 12.5% would lead to a breakdown of the magnetic moment. This occurs for both, LAPW and ASW calculations, and is in perfect agreement with earlier investigations using various other band-structure methods as well as different approximations for the exchange and correlation potential (see discussion above). Due to the large volume reduction required to suppress magnetic order it can be concluded that this discrepancy to present experimental data is *not* just a small shortcoming of the LSDA, but a major problem, either for theory or experiment. Our ASW calculations find the magnetic state by about 0.73 mRy/formula unit (FU) lower in energy than the nonmagnetic state in perfect agreement with previous results.[19] Thus it remains fairly unclear why the experimental investigations yield a nonmagnetic ground state for the ideal ordered $B2$ structure.

A possible explanation for the discrepancy between theory and experiment can be found from the DOS (Fig. 2) and the respective charge densities (Fig. 3), which show a rather unusually small nearest-neighbor (nn) Fe-Al, but a rather large next-nearest-neighbor (nnn) Fe-Fe interaction. The Fe-e_g orbitals point to the nnn Fe and appear to be

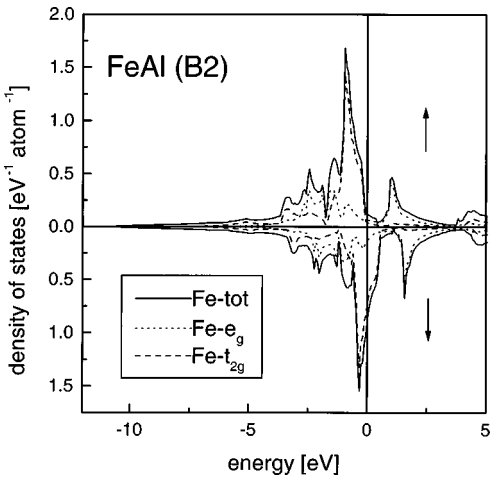

FIG. 2. Total and symmetry decomposed Fe DOS in FeAl ($B2$) obtained from ASW calculations.

broadened by the Fe-Fe interaction. Although the Fe-Fe distance is relatively large, these e_g states are split into a bonding and an antibonding part, where the latter is located 1.2 eV above the Fermi energy (E_F). In Fig. 3(a) the more localized $3d$ electrons pointing towards the next Fe are visible, but covalent Fe-Al contributions are hardly detectable. On the other hand the antibonding character with (almost) zero density between the atoms is evident [Fig. 3(c)]. The major peak in the DOS stems from Fe-t_{2g} states. These orbitals point towards the nn Al atoms, but despite the short bond length between Fe and Al only weak bonds are formed [Fig. 3(b)] and thus these states have a rather small energy dispersion. The DOS at E_F stems from these states and causes the Stoner criterion to be fulfilled so that the system spontaneously becomes ferromagnetically ordered. Due to the large energy separation between the antibonding e_g (which can carry two electrons) and the (nonbonding) t_{2g} states the d band can effectively accommodate only eight electrons. The spin-up t_{2g} band is filled so that Fe in FeAl behaves rather like Ni (with its almost filled d band). This similarity explains the unusual moment of about $0.7\mu_B$. If one decomposes the magnetic moment into its symmetry dependent contributions one finds that the major part of the magnetic moment originates from the t_{2g} electrons ($0.56\mu_B$) while the e_g electrons add only $0.12\mu_B$. Since these t_{2g} orbitals show a rather weak interaction with those of the neighboring atoms, any periodic substitution of neighboring atoms will have a minor effect on the magnetic moment. This conjecture was proven by (54-atom) supercell calculations in which the local environment of the central Fe atom was varied. Only if an Fe atom is surrounded by two shells of Al atoms it looses its magnetic moment. This result is also in agreement with the work by Guenzburger and Ellis,[42] who studied the magnetic state of Fe impurities in an $FeAl_{42}$ embedded cluster. The stability of the Fe moment with respect to variations in the nn environment is also found when a nine-atom Fe cluster in the center of the supercell is assumed even if the magnetic moments of the first neighboring shell change. In the next (undisturbed) nn Fe shell, however, the magnetic moments are back to the $0.7\mu_B$ that appear in the FeAl ($B2$) configuration.

Calculations for non-collinear-spin ordering were performed to study the dependence of the total energy on the

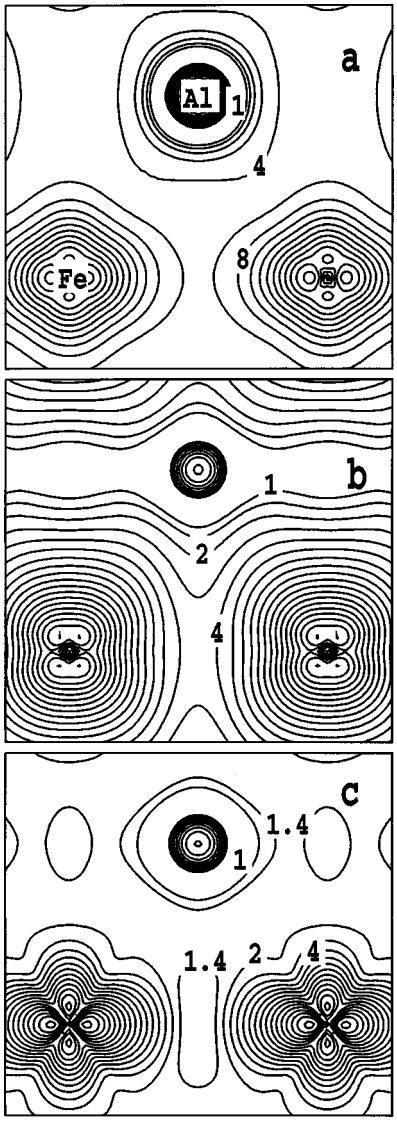

FIG. 3. Spin-up charge densities of FeAl ($B2$) in the (110) plane for (a) states from 4 to 1.75 eV below E_F (the bonding e_g-like states), (b) from 1.75 eV below E_F to E_F (the t_{2g} band) and (c) from E_F to 2.4 eV above E_F (the antibonding e_g band). The labels give the density in 0.01 $e/\text{Å}^3$.

formation of a spin spiral in various directions of the Brillouin zone.[39,43] The energy minimum is found for ferromagnetic spin alignment ($\mathbf{q}=0$) where $\mathbf{q}$ is the spin-spiral propagation vector [Fig. 4 (left)]. A rather strong dependence of the total energy E on $\mathbf{q}$ is found and whenever $E(\mathbf{q})$ exceeds approximately 1.2 mRy/FU the magnetic moments disappear and the system prefers to become nonmagnetic. Fitting the results to a Heisenberg model the spin-wave stiffness constant becomes very small (10.2 meV Å^2) leading to a roughly estimated Curie temperature of only 11 K. The application of a Heisenberg model, which is valid for systems with localized spins, seems justified, since the magnetic moments hardly change their value during the variation of the spin-spiral $\mathbf{q}$ vector.

B. Magnetic properties

Experimentally, we found that for sample 1 (Table I) above 30 K the temperature dependence of the susceptibility

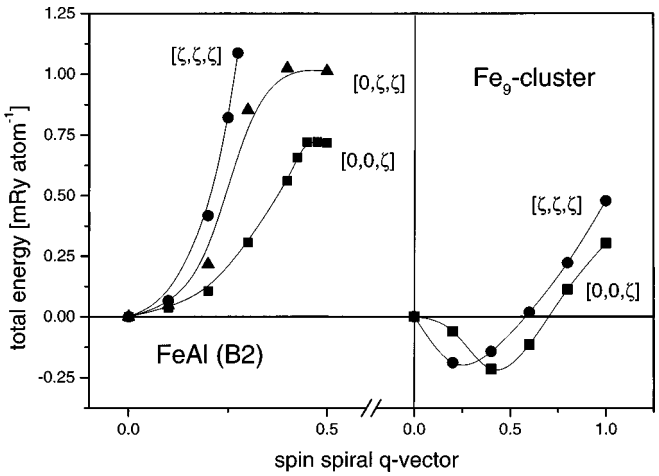

FIG. 4. Total energy for different spin-spiral vector directions in ideally ordered FeAl (left) and for a Fe_9Al_7 supercell (right).

derived from the magnetization measured at 6.62 T follows an extended Curie-Weiss behavior,

$$\chi=\chi_0+\frac{C}{T-\Theta} \tag{1}$$

(Fig. 5) with $C=9.63\times10^{-4}$ g^{-1} cm^3 K, $\chi_0=1.1\times10^{-5}$ g^{-1} cm^3, and $\Theta=1.8$ K. These values are in complete agreement with those reported in literature for samples with comparable composition and heat treatment (e.g., $C=9.9\times10^{-4}$ g^{-1} cm^3 K, $\chi_0=1.12\times10^{-5}$ g^{-1} cm^3, and $\Theta=-1.3$ K by Domke and Thomas[12]). The Mössbauer result, discussed below, shows, however, that for this sample only 25% of the Fe atoms (x_{MB}) carry a magnetic moment. Using this concentration one obtains an effective moment:

$$\mu_{\text{eff}}=2.83\sqrt{\frac{CM_A}{x_{\text{MB}}}}=1.13\mu_B \tag{2}$$

M_A is the atomic mass. By means of

$$\mu_{\text{eff}}=\sqrt{\mu(\mu+2)} \tag{3}$$

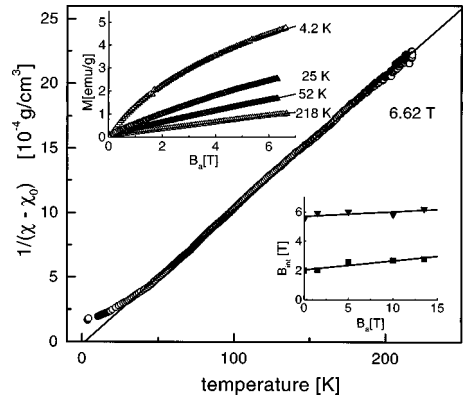

FIG. 5. Curie-Weiss contribution of the susceptibility for sample 1. The measurement was performed at 6.62 T. Inserts: magnetization of sample 1 at various temperatures. Field dependence of $B_{\text{int}}=|B_{\text{hf}}-B_a|$ obtained from the Mössbauer spectra of the single crystal (▼ Fe AS, ■ corner atoms around Fe AS).

one ends up with an averaged moment of $0.51\mu_B$ for the atoms in the nine-atom cluster.

Assuming a Langevin-type behavior at 4.2 K,

$$M=\chi_0 H+N\mu L\left(\frac{\mu H}{k_B T}\right), \tag{4}$$

the experimental data can be fitted with $N=1.54\times10^{20}\ \mathrm{g}^{-1}$, $\mu=3.43\mu_B$, $\chi_0=1.37\times10^{-5}\ \mathrm{g}^{-1}\,\mathrm{cm}^3$ (upper inset Fig. 5). Taking into account that the moment results from nine Fe atoms one obtains a mean moment of $0.38\mu_B$ per Fe atom, equivalent to an average effective moment of $0.95\mu_B$. From the resulting value of N one gets by this fitting procedure a concentration of 19.12% of magnetic Fe atoms. The resulting value for the Fe moment is in good agreement with that of the high-temperature extended Curie-Weiss fit, in which for the concentration of the magnetic atoms the Mössbauer results are used.

This Langevin-type fit holds also for the measurements at $T=25$ and 52 K with constant saturation magnetization of $N\mu=1.3\times10^{21}\mu_B\ \mathrm{g}^{-1}$. At 218 K the measured field dependence of the magnetization leads to $\mu_{\mathrm{eff}}=0.97\mu_B$, which is fairly close to the one obtained from the Curie-Weiss fit, where the Mössbauer result was used. In this case from the value of N follows that 19.14% of the Fe atoms carry a moment, which is in reasonably close agreement with the concentration of 25% decuced from Mössbauer measurements. Thus experimentally consistent results are obtained, if it is assumed that the measured moment results exclusively from the nine-atom Fe cluster.

To check for the magnetic properties of this cluster we performed band-structure calculations both for a smaller supercell with 16 atoms providing an effective composition of Fe_9Al_7 and for the 54-atom supercell where one Fe from a corner site was exchanged with the Al atom in the center of the unit cell thus keeping the nominal concentration of $Fe_{27}Al_{27}$ intact. Both calculations yield basically the same result. The magnetic moment at the central Fe atom is increased to about $1.7\mu_B$ whereas the moment of the surrounding eight Fe atoms is slightly reduced to $0.5\mu_B$. This yields an average moment of $0.63\mu_B$, which is comfortably close to the experimentally obtained $0.51\mu_B$ and the value proposed by Caskey, Franz, and Sellmyer[15] for the respective nine-atom cluster of $0.87\mu_B$.

C. Deconvolution of Mössbauer spectra

All recorded ^{57}Fe Mössbauer spectra could be analyzed with at least three subspectra: (i) a single unsplit line, (ii) one spectrum with a quadrupole splitting, and (iii) one that exhibits magnetic hyperfine splitting (B_{hf}) at 4.2 K (lower spectrum Fig. 6). These three subspectra can be attributed to distinct local environments of a ^{57}Fe probe atom, if one supposes that the above-mentioned defects, characteristic for the FeAl alloys, are randomly distributed[9] and takes into account nearest-neighbor exchange interactions only.

The unsplit line indicates vanishing quadrupole splitting. The CS value is the largest of all three subspectra. In the ideal $B2$ structure the EFG is zero because of symmetry reasons. Ignoring the formation of Al AS atoms Fe is surrounded by the largest number of Al atoms [Fig. 1(a)]. Thus this spectrum can be allocated to Fe situated in an undistorted $B2$ environment. A vacancy in the Fe sublattice leads to a local distortion of the eight surrounding cubes [Fig. 1(b)], causing an EFG. This is valid for the second subspectrum. The quadrupole splitting does not depend on temperature and is roughly the same within experimental accuracy for all investigated samples (Table I). An Fe AS atom is surrounded by eight nearest Fe neighbors as in bcc iron [Fig. 1(c)]. In the zero-field measurements only for the third subspectrum a hyperfine field is observed. The measured hyperfine field in the in-field experiments is always smaller than the applied one, and the CS value is the smallest (Table I). Therefore this should be the environment with the largest number of Fe neighbors. Consequently the CS values must be similar to those obtained for α-Fe, whereas for the Al-rich environment as found in the undistorted $B2$ structure a larger value for CS is expected from experiments, where Fe is embedded in various matrices [e.g., Ref. 44]. We conjecture that this third subspectrum can be allocated to the Fe AS and the eight surrounding Fe atoms.

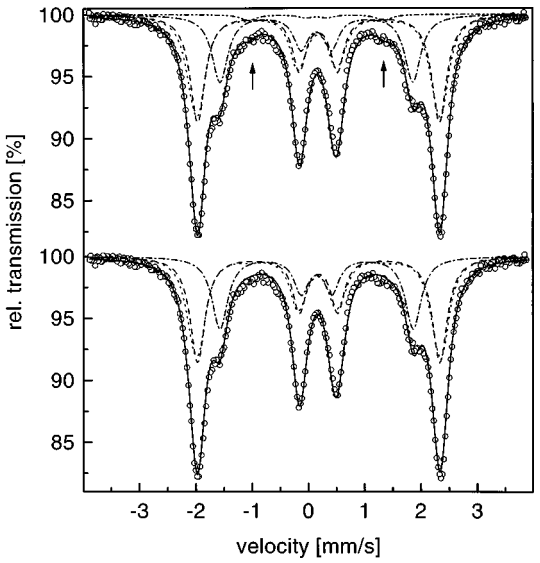

FIG. 6. ^{57}Fe Mössbauer spectra for sample 1 recorded at 4.2 K and 13.5 T fitted with three subspectra [Fe in ideally ordered $B2$ (dashed line), Fe around a Fe vacancy (dotted line), and Fe AS and corner atoms around Fe AS (dash-dotted line); lower spectrum] and with four subspectra [Fe in ideally ordered $B2$ (dashed line), Fe around a Fe vacancy (dotted line), corner atoms around Fe AS (dash-dotted line), and Fe AS (dash-dot-dot line); upper spectrum]. The arrows indicate the contribution of the Fe AS atom.

The remaining discrepancy between the measured and fitted spectrum and the recorded differences in moment for the central and the eight neighbor atoms[24] as well as the results of our supercell calculations encouraged us to subdivide the third subspectrum into two components representing the central atom (Fe AS) and the other eight surrounding Fe atoms, respectively. Thus the relative intensity ratio of these two subspectra was constrained to 1:8. The hyperfine splitting is according to the proposed large differences in moment quite different. This subdivision improves the final agreement (arrows, upper spectrum Fig. 6). A different analysis of spectra recorded at room temperature was performed by Collins and Peng[45] based on a local environment model and taking into

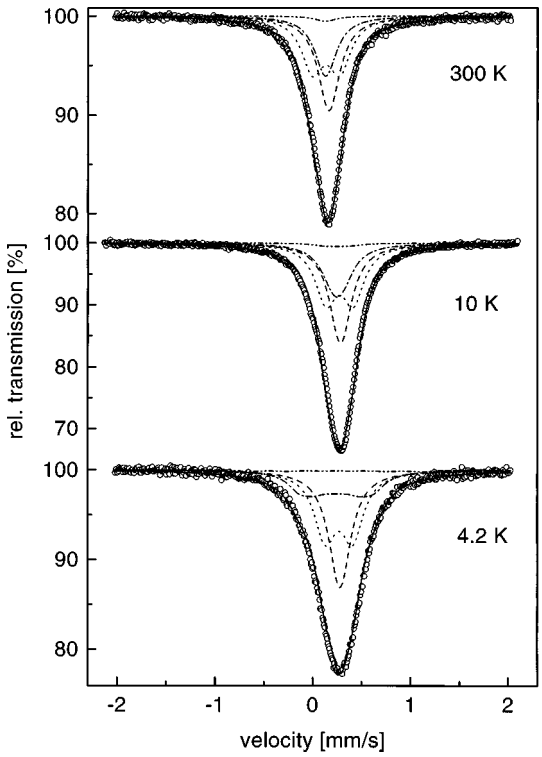

FIG. 7. ^{57}Fe Mössbauer spectra recorded at different temperatures without external field for sample 1 [Fe in ideally ordered $B2$ (dashed line), Fe around a Fe vacancy (dotted line), corner atoms around Fe AS (dash-dotted line), and Fe AS (dash-dot-dot line)].

account only monopol interactions, but ended up with defect concentrations two times larger than those obtained from x-ray measurements.[4]

Although the fits at 4.2 K with and without applied field and at room temperature are self-consistent, they are only unique with respect to the relative intensity caused by the eight neighbors of the Fe AS atom (Figs. 1 and 6). For the relative intensity of the remaining two subspectra uncertainties exist, which are due to the low resolution obtained in zero-field experiments. The sign of the principal axis of the EFG tensor was taken from the single-crystal measurements in an applied field (see discussion below). The FWHM values are either the same (sample 3) or slightly higher (max $+15\%$) for the crystal (sample 4) because of the larger thickness) than those obtained for the α-Fe calibration spectrum.

A precise determination of the disappearance of the hyperfine splitting of subspectrum 3 and 4 from the zero-field measurements was not possible. Above 50 K the same FWHM values were obtained as at room temperature. Below 50 K the FWHM values get slightly larger but still remain within an experimentally tolerable range for a single unsplit line. A significant increase is observed between 20 and 10 K and at 10 K the broadening caused by the hyperfine splitting is clearly visible (Fig. 7).

Above 1.5 T all spectra are fully polarized at 4.2 K. There is no intensity present at the $\Delta m=0$ transitions. Therefore internal fields acting at the ^{57}Fe nucleus can be calculated according to $B_{\rm int}=|B_{\rm hf}-B_a|$. For both the central Fe AS atom and the eight atoms at the corners of the surrounding cube $B_{\rm int}$ was found to increase with B_a (lower inset, Fig. 5). The slopes for the two sites are slightly different. The values extrapolated to vanishing B_a are in complete agreement with those determined from the zero-field measurements (2.0, 5.5 T) at the same temperature.

For the nine-atom Fe cluster embedded in the 16-atom supercell a non-collinear-spin order was allowed similar to the ordered $B2$ structure discussed above. The resulting ground state is not ferromagnetic but forms a spin helix along the [001] direction with a propagation vector of $[000.4]2\pi/a$, where a is the lattice constant of the supercell [Fig. 4 (right)]. In terms of the angles between Fe atoms in adjacent planes along the [001] direction that means that from plane to plane the spin direction is rotated by about 36°. This new magnetic state is 0.1 mRy/atom more stable than the ferromagnetic solution. It is surprising to see that also for a propagation along the [111] direction such a minimum is found that, however, is slightly less stable than the one discussed above.

Due to the small stabilization energy we can readily assume that in an applied field of a few T the spin will already be aligned and forced into the ferromagnetic ground state so that this noncollinear ground state will only be detectable at very small external fields. Furthermore it should be noted that our calculation assumes an infinite crystal with an undisturbed periodic array of supercells. The spin helix has a wavelength of about five lattice constants and thus requires to form at least an undisturbed ensemble of about 2000 atoms. Since the concentration of defects is of the order of a few percent they could easily suppress the formation of such a long-range interaction.

D. Quadrupole splitting

For the single crystal, which was mounted in the experimental setup in such a way, that the [111] direction coincided with the γ-ray direction (maximal deviations $\pm 2°$), the only fits consistent with the room-temperature measurements and the in-field experiments at 4.2 K gave an angle β of 75° between the γ-ray direction and principal axis of the EFG tensor (V_{zz}) for the Fe vacancy environment. The sign of V_{zz} is negative (Table I). The angle between [111] (and all equivalent directions) and the γ-ray direction [111] is 70.5°. This is within the experimental accuracy (precision of both cutting perpendicular to [111] and orientation of the surface with respect to the γ-ray direction) close to 75°. Thus experimentally a mean EFG tensor for the 26 atoms of the eight Fe cubes surrounding the vacancy oriented with the main axis along the body diagonals can be proposed. Because of the used radiation, no information about the two other components of the EFG tensor is available from the present experiments. The obtained value of the quadrupole splitting is close to the one reported for a similar environment of Fe in CoGa alloys.[46] For an Fe AS atom symmetry considerations exclude the presence of an EFG, however, for the eight surrounding atoms an EFG should lead to a quadrupole interaction. The spectral area of the former component is too low for a precise determination. For the latter no improvement of the fits were obtained if this interaction was taken into account, but we can exclude a large quadrupole splitting.

We have performed extensive EFG calculations using the LAPW method for Fe atoms around an Fe vacancy using supercells with 16, 32, and 54 atoms, both with and without spin polarization, and allowing for a full relaxation of all

TABLE II. EFG's [$eQV_{zz}/4$ in mm/s using $Q(^{57}\mathrm{Fe})=0.16$ b (Ref. 53)] on Fe atoms around an Fe vacancy in various supercells determined by means of non-spin-polarized (*n*) and spin-polarized (*sp*) LAPW calculations.

	n-Fe_7Al_8	n-$Fe_{15}Al_{16}$	n-$Fe_{26}Al_{27}$	sp-$Fe_{15}Al_{16}$
$Fe_{[100]}$	−0.079	+0.037	+0.009	−0.022
$Fe_{[110]}$	−0.047	+0.101	−0.050	+0.111
$Fe_{[111]}$			−0.002	

atomic positions. The results are summarized in Tables II and III. It is striking that even for the relatively large supercells no convergence of the EFG with respect to supercell size has been found. Instead, the EFG's depend strongly on the cell size and the ordering of the Fe vacancies. In the smallest cell, the nearest Fe atoms ($Fe_{[100]}$) sit between two vacancies and a strong negative EFG pointing towards the vacancies is found. However, in the 32-atom supercell the vacancies are ordered fcc-like (nearest vacancies in [110] direction) and the $Fe_{[100]}$-EFG changes sign and is much smaller, while the $Fe_{[110]}$ atom, which is now located between two vacancies, has a large positive EFG with large η pointing towards the vacancy. The differences between spin-polarized and non-spin-polarized results are small. In the largest supercell the Fe vacancies are already separated by three lattice parameters, but the EFG's have changed again considerably. Furthermore it must be noted, that even the largest EFG on $Fe_{[110]}$ is almost a factor of 3 smaller than the experimentally observed splitting. Thus with the present supercell sizes we cannot come to decisive conclusions explaining the experimental EFG.

The calculated EFG's are very sensitive to lattice relaxations and thus in all supercells we optimized the atomic positions. We find a small (about 1% of the undistorted distance) outward relaxation of the nearest-neighbor Al atoms but a significantly larger (1.7–3.5 %) one of the nearest $Fe_{[100]}$ atoms (also away from the vacancy). This is partly in contrast to other calculations, which yield even the opposite direction for Al (Ref. 31) or only a negligible small relaxation for both sites,[32] but it is consistent with the explanation of the DOS, which shows a particular strong Fe-Fe nnn interaction (see Sec. IV A). Note, that in the 54-atom cell significant relaxations even for the third and fourth shell of Fe and Al atoms around the vacancy are found indicating that larger supercells are necessary.

We have also investigated 16- and 32-atom supercells simulating an Fe-antisite defect. The resulting EFG for the Fe AS atom is zero by symmetry and for the nearest neighbors $Fe_{[111]}$ it is small (+0.023 mm/s) in agreement with experimental findings. The $Fe_{[111]}$ atoms relax towards the Fe AS by about 3% in agreement with Ref. 32 but in disagreement with Ref. 31.

TABLE III. Relaxations of neighboring atoms (in %, a negative sign means relaxation towards the vacancy) around an Fe vacancy in various supercells following from *n* and *sp* LAPW calculations.

	n-Fe_7Al_8	n-$Fe_{15}Al_{16}$	n-$Fe_{26}Al_{27}$	sp-$Fe_{15}Al_{16}$
$Al_{[111]}$	+1.3	+1.3	+0.8	+0.8
$Fe_{[100]}$		+1.7	+3.8	+2.8
$Fe_{[110]}$			−1.2	
$Fe_{[111]}$			+1.0	

E. Defect concentrations

As mentioned above the relative intensity of an individual subspectrum used in the analysis of the Mössbauer spectra is a direct measure of the number of Fe atoms incorporated in distinct environments. This is valid if one assumes that the Lamb-Mössbauer factors do not depend on these environments, which is quite reasonable for a metal. Thus the intensity of the single line spectrum represents the amount of undistorted $B2$ structure [Fig. 1(a)]. A single Fe vacancy distorts the *sp* configuration of the eight surrounding Al neighbors leading to both a change of their position and a redistribution of the bonding charge densities to their Fe neighbor atoms [Fig. 1(b)]. Therefore at least eight neighboring lattice cells (6, 12, and 8 atoms in [100], [110], and [111] and equivalent directions, respectively) are influenced. This distortion leads to the EFG at the Fe nucleus, observed in the second subspectrum. To estimate the value for the concentration of vacancies in the Fe sublattice the intensity of this subspectrum should be divided by 26. The magnetically hyperfine split subspectrum with the small intensity is allocated to the Fe AS atoms. The eight Fe atoms surrounding the Fe AS atom [Fig. 1(c), Table I] contribute to the intensity of the second magnetically hyperfine split spectrum [Fig. 1(c)]. Since the agreement between measured and fitted spectra is excellent, a further increase in the number of subspectra is not needed. The presence of Al AS atoms and Al vacancies cannot be excluded, their concentration, however, must be below the experimental resolution of the present Mössbauer measurements. It should be mentioned that in the present investigation all measurements are performed at low temperatures, where diffusion processes are extremely low. Thus the defect structure frozen in by the quenching process can be expected to be unaltered during the measuring time.

The Fe AS and vacancy concentrations are obtained within the present model for samples, which are quenched from various temperatures, and are compared in Fig. 8 with those reported in the literature. Since for the single crystal the cooling rate was not precisely determined, the quenching temperature is marked by an interval in this figure. For the two samples 6 and 7 in Table I measured after melt spinning without any heat treatment both the temperature and the cooling rate can only be roughly estimated. The possible range for the quenching temperature of these samples is also indicated. The agreement of the temperature dependence of the Fe AS concentration with the zero-field Mössbauer measurements performed at high temperature[10] is satisfactory. Generally the values based on magnetic measurements[47] are higher. In contrast to the present Mössbauer experiments a precise subdivision into the contribution resulting from center and corner atoms is not possible. Thus the obtained Fe AS concentrations are extremely dependent on the chosen mean cluster moment, which differs in the literature roughly by a factor of 2.[11,12,15,25]

The obtained low vacancy concentrations for the as cast melt spun samples are in agreement with investigations on

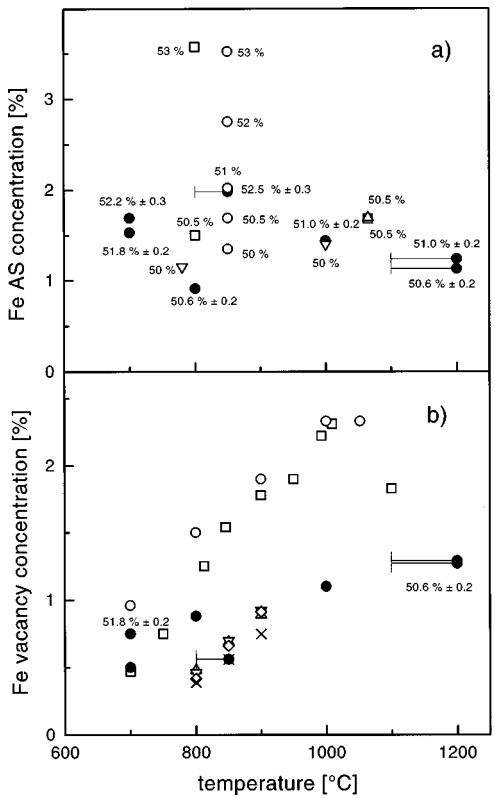

FIG. 8. Comparison of the deduced (a) Fe AS concentration (●) with those reported by Krachler *et al.* (Ref. 30) (□), Haberkern (Ref. 47) (○), Vogl and Sepiol (Ref. 10) (△), and Frantz (Ref. 25) (▽) and (b) vacancy concentration (●), with those reported by Ho and Dod (Ref. 50). [$x=0.49$ (△), 0.50 (▽), 0.515 (◇), and 0.53 (×)] and Paris and Lesbats (Ref. 48) [$x=0.49$ (□), quenched from the shown temperature and measured at 425 °C, and (○) measured at the indicated temperature]. The figures represent the Fe concentration [in (b) only those necessary to distinguish the samples are repeated]. The bars indicate the reasonable range of quenching temperatures for those three samples for which this temperature could not be directly measured.

other quenched and splat cooled samples for which the ordered atomic arrangement was found over the entire range of stability [Ref. 48 and references cited therein]. However, it must be kept in mind that FWHM values, as observed in the present experiments, can only appear if the hyperfine parameters for a certain surrounding of the ^{57}Fe probe atom remain unchanged. A large spread in these parameters (e.g., due to an increasing number of defects of quite different types) causes line broadening and increases the difficulty to separate these contributions from the background. Thus extremely irregularly arranged aggregates of defects may not be resolved in the present experiments. The agreement between our vacancy concentrations and the ones determined by other measuring techniques (x-ray and density,[4,48] dilatometry[49,50]) is, however, again satisfactory (Fig. 8).

Based on the assumption that only triple defects are present, Chang and Neumann[5] used a statistical-thermodynamic approach to derive equations for the concentration of vacancies and Fe AS atoms as a function of composition,

$$\Delta=\frac{z^3(1+\alpha-\alpha^2-\alpha^3)-\alpha^3(1+z-z^2-z^3)}{2z^2(1+\alpha-\alpha^2-\alpha^3)}, \qquad (5)$$

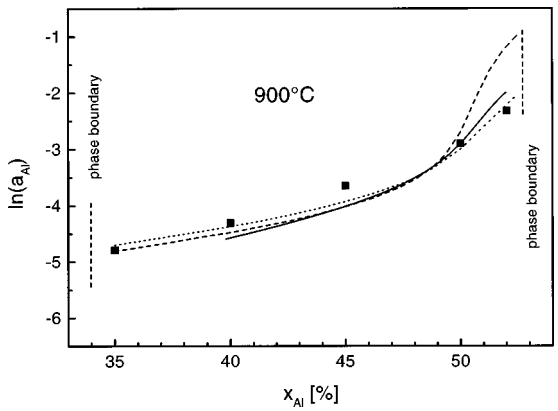

FIG. 9. Comparison of the concentration dependence of the activity (■) measured by Eldrige and Komarek (Ref. 51) with those calculated using $Q/R=4050$ K and $\ln a_{\mathrm{Al},0}=-3.0$ after Chang and Neumann (Ref. 5) (dotted line) and adapted $Q/R=5000$ K from the present Mössbauer measurements with $\ln a_{\mathrm{Al},0}=-3.0$ (dashed line), as well as from thermodynamic calculations taking into account Al vacancies with $\ln a_{\mathrm{Al},0}=-2.9$ (solid line).

where Δ defines the deviation from stoichiometry in terms of the mole fraction ($\Delta=x_{\mathrm{Al}}-0.5$), z is the vacancy concentration at Δ, and α is the disorder parameter (vacancy concentration at the exact stoichiometric composition $\Delta=0$). The temperature dependence of α was derived by these authors as

$$\alpha=\frac{1}{2^{2/3}}\exp\left[-\frac{Q}{RT}\right], \qquad (6)$$

where Q contains different enthalpy terms. Based on experimental data for the thermodynamic activity of aluminium, mainly by Eldridge and Komarek,[51] they determined $\alpha=2\times10^{-2}$ for a temperature of 900 °C (Fig. 9); this leads according to Eq. (6) to $Q/R=4050$ K (dotted line in Fig. 10). The results of the present experiments indicate that the temperature dependence of the defect concentrations (Fe vacancies and Fe AS atoms) is probably less pronounced. Increasing the value of Q/R to 5000 K would improve the situation (cf. Fig. 10), however, it would at the same time have a serious influence on the agreement between experimental aluminium activities and the resulting statistical-thermodynamic model curves especially on the Al-rich side (Fig. 9).

Earlier it had already been argued by Krachler, Ipser, and Komarek[41] that all four possible defects (vacancies and antistructure atoms on both sublattices) must be present in $B2$ phases, even if in many instances two of them exist in much higher concentrations than the other two (''triple defect'' and ''antistructure defect'' $B2$ phases[5]). Especially in the case of the Fe_xAl_{1-x} phase it turned out that the assumption of triple defects alone is not sufficient.

Optimizing the parameter set [see Eqs. (A11)] for the thermodynamic calculation with respect to the present experimental results yields for a temperature of 900 °C: $A=0.0074$, $B=0.0001$, $C=0.0168$. The corresponding activity curve is shown in Fig. 9 with a value of $\ln a_{\mathrm{Al},0}=-2.9$ (where $a_{\mathrm{Al},0}$, the aluminium activity at the exact stoichiometric composition, is an additional parameter). It can be seen that both model curves describe the experimental activity data more or less equally well.

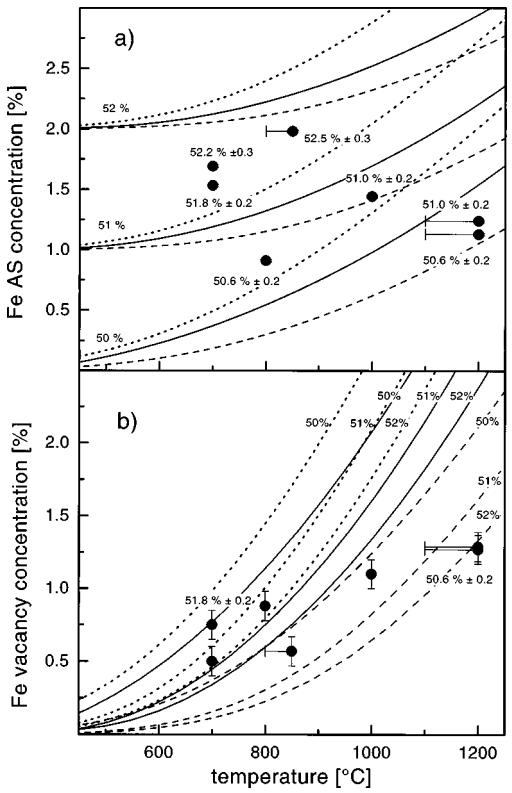

FIG. 10. Comparison of the measured temperature dependence of (a) the Fe AS and (b) Fe vacancy concentration (●) with thermodynamic model predictions based on triple defects using $Q/R = 4050$ K after Chang and Neumann (Ref. 5) (dotted line), and $Q/R = 5000$ K adapted to fit best to the present experiments (dashed line), as well as calculations allowing Al vacancies in addition (solid line). All three calculations were performed for 50, 51, and 52% Fe as indicated. For details see text.

Assuming that the sample compositions are correct within the error interval given in Table I, some of the existing discrepancies in Fig. 10 can be explained by uncertainties in the temperatures due to quenching problems: for example, in the samples 5 (1000 °C), 6, and 7 (1200 °C), where the calculated defect concentrations are considerably higher than the experimental ones, it is quite possible that the true equilibrium temperature should be 100–200 °C lower. Assuming for samples 6 and 7 that the equilibrium was frozen in at about 1000 °C instead of 1200 °C would result in a much better agreement. Such a failure to quench in the thermodynamic equilibrium at $T \geqslant 1000$ °C seems not to be unusual. In this respect it is not surprising that better agreement is observed for the samples, which had been quenched from $T \leqslant 850$ °C. On the other hand it is somewhat difficult to explain the differences for samples 1 and 2. For these it is interesting to note that the experimental Fe vacancy concentrations are too high whereas the Fe AS atom concentrations are too low compared with the calculated values. Nevertheless the agreement between the thermodynamic model and the microscopic picture used to explain the Mössbauer experiments is surprisingly good.

V. CONCLUSION

In agreement with band-structure calculations already reported in literature both the ASW and the LAPW calculations performed within this study lead also to a magnetic ground state for the ideal $B2$ structure. The resulting Fe moment of $0.71\mu_B$ remains stable for volume contractions below 12.5%, as long as the local environment up to the second-neighbor shell is not built up by Al only. The moment is caused by the large energy separation of the antibonding e_g states and the nonbonding t_{2g} states. The latter are responsible for the high DOS at the Fermi energy. This ground state is, however, only 0.7 mRy/FU below the paramagnetic state.

The discrepancy to the experiment, where, by high-field Mössbauer spectroscopy, it was found that (depending on concentration and heat treatment) only approximately 25% of the Fe atoms carry a magnetic moment whereas all others remain nonmagnetic, could be explained by means of calculations allowing non-collinear-spin ordering. Although the energy minimum appears again for ferromagnetic alignment, a strong dependence of the total energy on the spin-spiral propagation vector and a disappearance of the magnetic moments at energies above 1.2 mRy/FU is found. Thus the analysis of these band structure calculations allows to conclude that long-range magnetic order is not very stable even in an ideal $B2$ FeAl. The high density of defects that is found in real systems destroys the atomic periodicity and this lack of periodicity can cause a diminishing of the Fe moment.

Using the concentration of the magnetic Fe atoms derived from high-field Mössbauer spectroscopy, the fit of the temperature dependence of the susceptibility to an extended Curie-Weiss law leads to an averaged moment of $0.51\mu_B$. Assuming that the measured moment is caused by an Fe AS atom and the eight Fe nn atoms, one ends up with a mean moment per atom of this cluster of $0.38\mu_B$ and an overall concentration of 19% of magnetic atoms, if a Langevin-type behavior is proposed at 4.2 K for the field dependence of the magnetization. Supercell calculations (with both a 16- and a 54-atom supercell) yield $1.7\mu_B$ for the central Fe AS atom and $0.5\mu_B$ for the eight corner atoms resulting in an average moment of $0.63\mu_B$ for the cluster.

This good agreement between the two experiments and the supercell calculations strongly supports the microscopic model used to allocate the four subspectra in the Mössbauer analysis to distinct Fe environments. Two of these subspectra are due to Fe AS atoms and the eight surrounding atoms at the corners. The in-field Mössbauer measurements indicate that these atoms have a magnetic moment. The third subspectrum, which remains a single line even at 4.2 K and has $B_{\text{int}} = 0$ T in an applied field of 13.5 T represents the amount of undistorted $B2$ structure. The fourth, exhibiting a quadrupole but no magnetic hyperfine splitting, is allocated to Fe atoms surrounding a vacancy in the Fe sublattice. V_{zz} of this mean EFG points in the direction of the body diagonals and has a negative sign. Unfortunately this microscopical picture could not be supported by the present LAPW calculations, which may suffer from too small supercells, but also from some deficiencies of the LSDA, which lead to ferromagnetic order in contrast to experiment and which may also influence the charge distribution and thus the EFG. For the eight corner atoms around the Fe AS atom a quadrupole splitting could exist, which, however, is not observed in the experiment. The calculated value for this V_{zz} is smaller than the one obtained for the Fe atoms surrounding a vacancy and might thus be beyond the experimental resolution.

The great advantage of the performed Mössbauer experiments is that simultaneously the concentration of both the Fe vacancies and the Fe AS atoms is obtained from the intensities of the subspectra restricting the analysis to nn interactions. This restriction does not seem to be crucial, since ASW calculations yield an attenuation of the influence of any defect on the value of the moment within short spatial distances, if the periodic arrangement of the atoms in a $B2$ structure is kept unchanged in the surrounding shells. The subspectra due to Fe AS contributions are fully resolved, and therefore one does not need to precisely know the cluster moment, which is in contrast to the determination of the Fe AS concentrations based on bulk magnetic measurements. The agreement of the derived vacancy concentration with the one reported in the literature is satisfactory. The temperature dependence of both, the Fe AS and the vacancy concentration agrees well with thermodynamic model calculations allowing vacancies on both lattice sites and is less pronounced than that reported for pure triple defects. It should be stressed that both the microscopic model (proposed to calculate the defect concentrations from the Mössbauer subspectra associated with certain environments) and the thermodynamic calculations are based on the assumption that the defects are isolated. Concerning these model calculations, it seems to be of increasing importance to consider all possible kinds of point defects. Finally it must be mentioned that the evolved microscopic model not only works to explain the magnetic measurements, but is also capable of explaining reasonably well thermodynamic results like the activity.

ACKNOWLEDGMENTS

This work is partly supported by the Austrian FWF (Project No. S5604 and S5601) and the Jubiläumsfonds of the Austrian National Bank (Project No. 5736).

APPENDIX

The calculations of the defect concentrations within the statistical-thermodynamic model are based on a mean-field approximation similar to that used by Chang and Neumann.[5] Implementation of the Wagner-Schottky approach[52] makes the calculations less complicated, since the following partial derivatives of the internal energy are assumed to be constants:

$$\left(\frac{\partial U}{\partial N_A^\beta}\right)_{\mu_A,\mu_B,N^g,T,N_B^\alpha,N_V^\beta,N_V^\alpha} = C_1, \tag{A1}$$

$$\left(\frac{\partial U}{\partial N_B^\alpha}\right)_{\mu_A,\mu_B,N^g,T,N_A^\beta,N_V^\beta,N_V^\alpha} = C_2, \tag{A2}$$

$$\left(\frac{\partial U}{\partial N_V^\alpha}\right)_{\mu_A,\mu_B,N^g,T,N_A^\beta,N_B^\alpha,N_V^\beta} = C_3, \tag{A3}$$

$$\left(\frac{\partial U}{\partial N_V^\beta}\right)_{\mu_A,\mu_B,N^g,T,N_A^\beta,N_B^\alpha,N_V^\alpha} = C_4, \tag{A4}$$

where μ_A and μ_B are the chemical potentials of the two components A and B (Fe and Al), N^g is the total number of lattice sites, N_A^β and N_B^α are the numbers of antistructure atoms on the two sublattices, N_V^β and N_V^α are the numbers of vacancies on the two sublattices.

The model calculations yield the distribution of atoms and vacancies on the two sublattices:

$$\frac{N_A^\alpha}{N^g} = \frac{\frac{1}{2}\exp(C_3N_L/RT)}{\exp(-\mu_A/RT)+\exp(C_3N_L/RT)+\exp(\mu_B/RT-C_2N_L/RT+C_3N_L/RT-\mu_A/RT)}, \tag{A5}$$

$$\frac{N_B^\alpha}{N^g} = \frac{\frac{1}{2}\exp(\mu_B/RT-C_2N_L/RT+C_3N_L/RT-\mu_A/RT)}{\exp(-\mu_A/RT)+\exp(C_3N_L/RT)+\exp(\mu_B/RT-C_2N_L/RT+C_3N_L/RT-\mu_A/RT)}, \tag{A6}$$

$$\frac{N_V^\alpha}{N^g} = \frac{\frac{1}{2}\exp(-\mu_A/RT)}{\exp(-\mu_A/RT)+\exp(C_3N_L/RT)+\exp(\mu_B/RT-C_2N_L/RT+C_3N_L/RT-\mu_A/RT)}, \tag{A7}$$

$$\frac{N_A^\beta}{N^g} = \frac{\frac{1}{2}\exp(\mu_A/RT-C_1N_L/RT+C_4N_L/RT-\mu_B/RT)}{\exp(-\mu_B/RT)+\exp(C_4N_L/RT)+\exp(\mu_A/RT-C_1N_L/RT+C_4N_L/RT-\mu_B/RT)}, \tag{A8}$$

$$\frac{N_B^\beta}{N^g} = \frac{\frac{1}{2}\exp(C_4N_L/RT)}{\exp(-\mu_B/RT)+\exp(C_4N_L/RT)+\exp(\mu_A/RT-C_1N_L/RT+C_4N_L/RT-\mu_B/RT)}, \tag{A9}$$

$$\frac{N_V^\beta}{N^g}=\frac{\frac{1}{2}\exp(-\mu_B/RT)}{\exp(-\mu_B/RT)+\exp(C_4N_L/RT)+\exp(\mu_A/RT-C_1N_L/RT+C_4N_L/RT-\mu_B/RT)}, \tag{A10}$$

where N_L is Avogadro's constant.

Our model parameters are the point defect concentrations in the exactly stoichiometric alloy at the temperature T:

$$a=\left(\frac{N_A^\beta}{N^g}\right)_{\text{stoich}}, \quad b=\left(\frac{N_B^\alpha}{N^g}\right)_{\text{stoich}}, \quad c=\left(\frac{N_V^\alpha+N_V^\beta}{N^g}\right)_{\text{stoich}} \tag{A11}$$

[1] Y. A. Chang, L. M. Pike, C. T. Liu, A. R. Bilbrey, and D. S. Stone, Intermetallics **1**, 107 (1993).
[2] D. G. Morris, J. C. Joye, and M. Leboeuf, Philos. Mag. A **69**, 961 (1994).
[3] K. Yoshimi, S. Hanada, and H. Tokuno, Mater. Trans., JIM **35**, 51 (1994).
[4] H. Xiao and I. Baker, Acta Metall. Mater. **43**, 391 (1995).
[5] Y. A. Chang and J. P. Neumann, Prog. Solid State Chem. **14**, 221 (1982).
[6] R. J. Wasilewski, J. Phys. Chem. Solids **29**, 39 (1968).
[7] M. B. Stearns, J. Appl. Phys. **35**, 1095 (1964).
[8] G. P. Huffman and R. M. Fisher, J. Appl. Phys. **38**, 735 (1967); R. B. Frankel, D. J. Sellmyer, and N. A. Blum, Phys. Lett. **33A**, 13 (1970).
[9] R. Wagoner, M. Reissner, W. Steiner, J. Bogner, H. Sassik, P. Pongratz, and B. Sepiol, J. Magn. Magn. Mater. **140-144**, 57 (1995); W. Steiner, M. Reissner, J. Bogner, H. Sassik, and B. Sepiol, Hyperfine Interact. **1**, 372 (1996).
[10] G. Vogl and B. Sepiol, Acta Metall. Mater. **42**, 3175 (1994).
[11] W. Köster and T. Gödecke, Z. Metallkd. **71**, 765 (1980); **72**, 707 (1981); **73**, 111 (1982); **73**, 502 (1983); W. Köster, E. Wachtel, and T. Gödecke, *ibid.* **76**, 382 (1985); **76**, 676 (1985).
[12] H. Domke and L. K. Thomas, J. Magn. Magn. Mater. **45**, 305 (1984).
[13] M. Höhl, Z. Metallkd. **51**, 85 (1960).
[14] A. Parthasarathi and P. A. Beck, Solid State Commun. **18**, 211 (1976).
[15] G. R. Caskey, J. M. Franz, and D. J. Sellmyer, J. Phys. Chem. Solids **34**, 1179 (1973).
[16] R. Podlucky and A. Neckel, Phys. Status Solidi B **95**, 541 (1979).
[17] C. Blaas, J. Redinger, S. Manninen, V. Honkimäki, K. Hämäläinen, and P. Suortti, Phys. Rev. Lett. **75**, 1984 (1995).
[18] Ch. Müller, H. Wonn, W. Blau, B. Ziesche, and V. B. Krivitskii, Phys. Status Solidi B **95**, 215 (1979).
[19] B. I. Min, T. Oguchi, H. J. F. Jansen, and A. J. Freeman, J. Magn. Magn. Mater. **54-57**, 1091 (1986).
[20] R. Eibler and A. Neckel, J. Phys. F **10**, 2179 (1980).
[21] G. A. Botton, G. Y. Guo, W. M. Temmerman, and C. J. Humphreys, Phys. Rev. B **54**, 1682 (1996).
[22] V. Sundarajan, B. R. Sahu, D. G. Kanhere, P. V. Panat, and G. P. Das, J. Phys.: Condens. Matter **7**, 6019 (1995).
[23] H. Chachan, E. G. da Silva, D. Guenzburger, and D. E. Ellis, Phys. Rev. B **35**, 1602 (1987).
[24] Y. M. Gu and L. Fritsche, J. Phys.: Condens. Matter **4**, 1905 (1992).
[25] W. Frantz, thesis, Max-Planck-Institut, Stuttgart, 1994.
[26] R. Feldwisch, B. Sepiol, and G. Vogl, Acta Metall. Mater. **43**, 2033 (1995).
[27] J. P. Neumann, Y. A. Chang, and C. M. Lee, Acta Metall. **24**, 593 (1976).
[28] C. Y. Cheng, P. P. Wynblatt, and J. E. Dorn, Acta Metall. **15**, 1045 (1967).
[29] C. Kinoshita and T. Eguchi, Acta Metall. **20**, 45 (1972).
[30] R. Krachler, H. Ipser, B. Sepiol, and G. Vogl, Intermetallics **3**, 83 (1995).
[31] C. L. Fu, Y.-Y. Ye, M. H. Yoo, and K. M. Ho, Phys. Rev. B **48**, 6712 (1993); C. L. Fu, *ibid.* **52**, 3151 (1995).
[32] J. Mayer, C. Elsässer, and M. Fähnle, Phys. Status Solidi B **191**, 283 (1995).
[33] G. Bozzolo, J. Ferrante, R. D. Noebe, and C. Amador, Scr. Metall. **36**, 813 (1997).
[34] J. R. Gabriel and S. L. Ruby, Nucl. Instrum. Methods **36**, 23 (1965).
[35] S. Mørup and E. Both, Nucl. Instrum. Methods **124**, 445 (1975).
[36] P. Blaha, K. Schwarz, and J. Luitz, WIEN97, Vienna University of Technology 1997 [Improved and updated UNIX version of P. Blaha, K. Schwarz, P. Sorantin, and S. B. Trickey, Comput. Phys. Commun. **59**, 399 (1990)].
[37] A. R. Williams, J. Kübler, and C. D. Gelatt, Jr., Phys. Rev. B **19**, 6094 (1979).
[38] J. P. Perdew, S. Burke, and M. Ernzerhof, Phys. Rev. Lett. **77**, 3865 (1996).
[39] L. M. Sandratskii, Solid State Commun. **75**, 527 (1990).
[40] R. Krachler and H. Ipser, Intermetallics (to be published December 1998).
[41] R. Krachler, H. Ipser, and K. L. Komarek, J. Phys. Chem. Solids **50**, 1127 (1989); **51**, 1239 (1990).
[42] D. Guenzburger and D. E. Ellis, Report No. CBPF-NF-023/91.
[43] P. Mohn, K. Schwarz, M. Uhl, and J. Kübler, Solid State Commun. **102**, 729 (1997).
[44] A. M. Van der Kraan and K. H. J. Buschow, Physica B **138**, 55 (1986).
[45] G. S. Collins and L. S. J. Peng, Nuovo Cimento D **18**, 329 (1996).
[46] G. L. Whittle, P. E. Clark, and R. Cywinski, J. Phys. F **10**, 2093 (1980).
[47] M. R. Haberkern, thesis, Max-Planck-Institut, Stuttgart, 1990.
[48] D. Paris and R. Lesbats, J. Nucl. Mater. **69 & 70**, 628 (1978).
[49] J. P. Riviere, Mater. Res. Bull. **12**, 995 (1977).
[50] K. Ho and R. A. Dodd, Scr. Metall. **12**, 1055 (1978).
[51] J. Eldrige and K. L. Komarek, Trans. Metall. Soc. AIME **230**, 226 (1964).
[52] C. Wagner and W. Schottky, Z. Phys. Chem. Abt. B **11**, 163 (1931).
[53] Ph. Dufek, P. Blaha, and K. Schwarz, Phys. Rev. Lett. **75**, 3545 (1995).